Journal of Directed Energy, 2, Spring 2007, 189–209

Using Defocus to Improve Peak Irradiance for Air-to-Ground High-Energy Laser Weapons

Scott N. Long* **and J. O. Miller**

Air Force Institute of Technology, Wright–Patterson Air Force Base, Ohio 45433

Robert T. Brigantic

Pacific Northwest National Laboratory, Richland, Washington 99352

and

Matthew E. Goda

Air Force Research Laboratory, Wright–Patterson Air Force Base, Ohio 45433

Chemical oxygen-iodine laser (COIL)–based weapon systems that operate near the ground will experience thermal blooming due to atmospheric absorption if output power is sufficiently high. The thermal lens in the air-to-ground case is predominantly in the far field of the optical system, which puts the problem outside the envelope for most classical phase correction techniques. Focusing the laser beyond the target (defocus) in the air-to-ground regime is shown to improve irradiance at the target and can be thought of as reducing the thermal blooming distortion number N_D rather than as phase correction. Improvement is shown in a baseline scenario presented and all variations from it are explored. The Breaux N_D is examined for potential use in a defocus scaling law, and a correction factor due to Smith is proposed to address deficiencies. Optimal defocus settings and expected improvement are presented as a function of Breaux N_D, and a discussion of the interaction between turbulence and thermal blooming that may limit performance in the air-to-ground case is given.

KEYWORDS: Chemical oxygen-iodine laser, High-energy laser, Strehl improvement, Thermal blooming, Turbulence

Nomenclature

a_i	initial radius of the laser beam at the propagating aperture
a_f	final radius of the laser spot at the target for the given degree of focus as well as diffraction and other linear effects
a_{geom}	ray-optics radius of the beam at given point along optical path
c_P	specific heat of atmosphere

Received February 2, 2006; revision received October 19, 2006.

*Corresponding author: e-mail: Scott.Long@RANDOLPH.AF.MIL.

k	wave number (2π divided by wavelength)
N_D	thermal blooming (phase) distortion number
N_{focus}	focus adjustment multiple for N_D
n_0	unperturbed refractive index of air
P	laser output power at aperture
R_{target}	distance from the aperture to the target plane
S_{interact}	Strehl ratio for the interaction of turbulence and thermal blooming effects
S_{TB}	Strehl ratio for thermal blooming effect in absence of turbulence
$S_{\text{TB+turb}}$	Strehl ratio for combined effect of turbulence and thermal blooming
S_{turb}	Strehl ratio for turbulence effect in absence of thermal blooming
s	spread of the beam at given point on optical path due to diffraction and beam quality effects as well as specialized estimate of the spread due to blooming
T	atmospheric temperature at given altitude
T_0	atmospheric baseline temperature (300 K, for this research)
V_E	effective wind velocity perpendicular to optical path
α_{abs}	absorption coefficient
α_{scat}	scattering coefficient
$\partial n/\partial T$	rate-of-change refractive index with respect to local temperature
ρ	air density
τ	transmission (fraction of power transmitted over a given optical path)

1. Introduction

The Department of Defense is developing a concept demonstrator of a high-energy laser (HEL) air-to-ground weapon called the Airborne Tactical Laser (ATL). The ATL is being constructed with a chemical oxygen-iodine laser (COIL), which operates at a wavelength of 1.315 μm. Unfortunately, although COIL devices can generate high laser powers for propagation, 1.315-μm light is readily absorbed by any water vapor in the atmospheric path. This absorption reduces the laser power that reaches the target, and if the atmospheric heating that accompanies the absorption is severe enough, the beam will also become distorted by resulting air density fluctuations in the optical path in a process called thermal blooming. Thermal blooming distortion usually reduces the peak irradiance of the laser spot at the target. One possibility for mitigating this effect of thermal blooming for a given engagement scenario is to focus the beam at a point beyond the target during propagation rather than directly at the target. When thermal blooming is a significant effect, the marginal reduction in the thermal blooming distortion is often a stronger function of relative defocus than is the defocusing effect itself on peak irradiance in the absence of absorption. When this is the case, peak irradiance of the laser spot at the target will rise, then crest, and then fall as a function of relative defocus. Thus, in many thermal blooming conditions, an appropriate amount of defocus should improve the overall peak irradiance at the target over the focused case.

Defocus has been known for some time to be a primary contributor to correction for thermal blooming in the presence of convection.[1,9] Typically, defocus is discussed as a portion of the optical wavefront correction. Wavefront correction implies that wavefront aberrations near the transmitting aperture are the subject of interest in those articles, since phase correction is less effective as the aberrations occur at increasing distances from the aperture. In the air-to-ground case, however, most of the thermal blooming aberration occurs far from the aperture since the weapon platform is moving at aircraft velocities (high

effective wind velocities reduce thermal blooming near the aperture) in less absorptive air at altitude, and the target on the ground is stationary in our case, though subject to wind, and in a more absorptive atmosphere. In view of this, we find it valid to think of defocus not as a wavefront correction, but as a method to reduce the thermal blooming distortion number N_D as compared to the focused case, with the resulting improvement in the Strehl ratio due to thermal blooming.

Further, it would be useful to know the conditions under which defocusing the beam will be beneficial to increasing peak irradiance of the laser spot on target, and when these conditions are met, knowledge of the optimal defocus distance, as well as the expected peak irradiance itself, will be important. Not surprisingly, these results are highly multivariate functions of the engagement scenario, depending on, for example, atmospheric absorbance and scatter, optical path wind profile, laser power and beam profile, aperture specifications, range to target, and strength of turbulence. Wave optics simulations that account for these variables have been available for many years to study thermal blooming and other atmospheric effects. For this study we are using Science Applications International Corporation's (SAIC's) Atmospheric Compensation Simulation (ACS). ACS is a Fortran-based code written and maintained by Donald Link[10] that can run on UNIX, LINUX, or Windows platforms. The scenario and the weapon systems parameters are read by ACS from a text file, and in addition to these settings, many parameters have to be established, including numbers and resolution of phase screens, number of replications to average, simulation time step, dwell time, and delay before gathering statistics. Output files include the irradiance profiles at the target, with and without atmospheric distortions, and summary statistics for the engagement.

The important finding for this paper is that all operating conditions studied herein benefited in terms of peak irradiance from having some amount of defocus. Since operating with a focused beam is an arbitrary decision (at least in the presence of thermal blooming), it should be relatively inexpensive to add defocusing capability to existing designs or operating procedures. Also, since other effects may cause beam spreading in ATL scenarios, such as diffraction due to aerosols[16] or aero-optic effects at the beam turret, we may find that weapons operated at thermal blooming wavelengths are not negatively impacted by these phenomena if the spreading effects are no larger than the spreading associated with optimal defocus. On the other hand, we note that time-averaged spreading due to turbulence does not always mitigate the thermal blooming effect, and often worsens it.

To illustrate these findings, the Breaux thermal blooming distortion number N_D is reviewed and a baseline scenario is defined. We then examine the sensitivity of system performance in many dimensions of the scenario, which shows how much defocus is advisable and how much improvement might be gained. Next we explore a proposed modification to the Breaux N_D that could make defocus an added feature in scaling laws that use the Breaux N_D. Finally, we observe that thermal blooming interacts with turbulence in ways that can affect the optimal defocus and further limit the performance of HEL systems beyond the effects of thermal blooming and turbulence independently.

2. Thermal Blooming Distortion Number

Historically, the effect of thermal blooming has been discussed with respect to the thermal blooming distortion number N_D. N_D is designed to be a scaling variable that is correlated to blooming effect and that relates the effect of engagement scenario parameters to each other. For example, according to the N_D formula [see Eq. (1) below], the effect of doubling

the wind (which reduces N_D) is the same as halving the power. There have been prominent scaling laws relating N_D to peak irradiance at the target plane that have been given by Smith,[18] Gebhardt,[7] and Breaux.[2] These relate N_D to the thermal blooming Strehl ratio S_{TB}—the ratio of peak irradiance with thermal blooming to peak irradiance with no thermal blooming (but including power loss due to absorption)—which is a decreasing function of N_D.

Origination of N_D is often attributed to Bradley and Herrmann,[1] though Gebhardt and Smith[8] had a similar construct. It was cast into integral form by Breaux,[2] among others (e.g., Ref. 13), and Breaux's was modified by Vernon and St. John[19] to explicitly include effective wind velocity V_E in the integrand rather than merely a scaling factor to account for slewing. Vernon and St. John also moved the absorption coefficient (α_{abs}) and temperature (T) under the integral since those will vary with altitude, an important dimension in the ATL case. Starting with Bradley and Herrmann and leveraging the others' developments, the formulation for N_D used in our research, then, is as follows:

$$N_D = \frac{kPT_0(-\partial n/\partial T)}{\rho c_P n_0} \int_0^{R_{target}} dr \frac{1-(r/R_{target})}{\sqrt{a_{geom}^2(r)+s^2(r)}} \cdot \frac{\alpha_{abs}(r)\tau(r)}{V_E(r)T(r)}, \tag{1}$$

where k is the wave number, P is the laser power, T_0 is a temperature baseline (300 K, for this research), $\partial n/\partial T$ is the rate-of-change refractive index with respect to local temperature, ρ is the air density, c_P is the specific heat of air, n_0 is the unperturbed refractive index of air, and R_{target} is the distance from the aperture to the target plane. The integration proceeds from the aperture to the target and, in addition to those functions mentioned earlier, the integrand consists of these functions of position along the optical path: a_{geom} is the ray-optics radius of the beam, s is a specialized function developed by Breaux[2] that contains the spread of the beam due to diffraction and beam quality effects as well as an estimate of the spread due to blooming (the latter added to improve correlation of his scaling law), and τ is the transmission. Vernon and St. John added turbulence and other linear effects to s in their modeling. Note in Eq. (1) that the contribution of each portion of the beam to N_D is inversely related to the beam size at that point. However, Breaux also recommends weighting each beam position by the proportion of the path remaining to the target (i.e., path leverage); hence the $1-(r/R_{target})$ in the numerator. Because of this as well as the inclusion of s, we will refer to Eq. (1) as the Breaux N_D formulation. We note that Bradley and Hermann rejected path weighting by leverage and beam size since those tend to cancel each other out in the focused case; this reasoning is superseded by inclusion of Breaux's spreading term.

We follow Vernon and St. John as well as Magee and Ngwele[13] in modeling the transmission function in Eq. (1) as follows:

$$\tau(r) = \exp\left\{-\int_0^r dr'[\alpha_{abs}(r') + \alpha_{scat}(r')]\right\}, \tag{2}$$

where α_{scat} is the scattering coefficient.

The construction of Eq. (1) suggests that it could be applied to defocused beams by modifying the beam size function a_{geom} to something other than the target-focused case. As we will show, however, it is not so simple. The difficulty lies in the special spreading function s, the estimated blooming portion of which appears to have been developed for the focused case. As a result, s dominates a_{geom} in the root sum squared (RSS) under the integral near the target for the defocused cases; this results in little change in calculated

N_D as a function of defocus. Since wave optics shows that defocus can result in significant improvement of peak laser intensity at the target in the air-to-ground case, the Breaux N_D equation (1) cannot be applied without modification in a scaling law that seeks to model the effect of beam defocus.

To overcome this limitation of the Breaux formulation, we leverage Smith,[18] who developed correction factors for various aspects of the collimated thermal blooming case under constant wind and low absorption assumptions. In particular, the correction factor derived for converting a collimated distortion number to that for a focused case is

$$N_{\text{focus}}(a_i/a_f) = \frac{2(a_i/a_f)^2}{(a_i/a_f - 1)}\left[1 - \frac{\ln(a_i/a_f)}{(a_i/a_f - 1)}\right], \tag{3}$$

where a_i is the radius of the propagating aperture and a_f is the radius of the spot at the target for the given degree of focus as well as diffraction and other linear effects (such as turbulence and jitter). Fitting our purpose, note that the focus distance, from which a_f is determined, need not be the same as the target distance but can be beyond it. However, since the Breaux formulation already assumes that the beam is focused at the target, determining N_D for a defocused (noncollimated) case requires first dividing Eq. (1) by Eq. (3) evaluated for the target-focused case and then multiplying by Eq. (3) reevaluated for the defocused case. N_D for defocused settings calculated in this way will be referred to as Breaux and Smith results. Results of this approach are discussed in a later section. Next, we describe a baseline air-to-ground HEL engagement scenario that is useful for evaluating our N_D formulation.

3. Baseline Scenario

To understand how a notional ATL will respond to defocus in view of the many factors that determine performance, we first establish a baseline air-to-ground scenario with two laser power values. We will later examine sensitivities and expand our scope. Here are the particulars of the baseline scenario:

- Weapon platform: 2-km altitude, 100-m/s due east velocity vector
- Target point: located east of platform, on ground at sea level, and stationary; 6,000-m slant range from platform
- Laser aperture: 0.5-m diameter, 30% single-axis central obscuration
- Atmosphere: 1976 U.S. Standard for temperature (Vernon and St. John); the Mani[14] atmosphere for absorption and scattering (molecular and aerosol), Bufton wind model with 10-m/s wind at ground from the north (Vernon and St. John). No turbulence is assumed for most of the analysis. When turbulence is included, the HV 5/7 atmosphere is assumed (Vernon and St. John).
- Laser powers at aperture: 50- and 100-kW continuous-wave, beam quality 1.0, uniform beam profile
- Beam control: closed-loop tracker for tilt correction only, no higher-order correction

While not part of the scenario in a real-world sense, an important part of any wave-optics simulation setup is phase screen selection and positioning. We found that the accurate modeling of thermal blooming can require additional phase screens beyond what is needed to model laser propagation in turbulence alone. For this scenario, 10 phase screens is adequate for modeling turbulence alone, but for also modeling thermal blooming, additional phase

Table 1. Average across focus ranges 6,000–7,500 m of magnitude percentage change in peak irradiance for each incremental increase in phase screen number

Phase screen change	Average change in peak irradiance, %
20 from 10	9.0
30 from 20	1.5
40 from 30	0.5

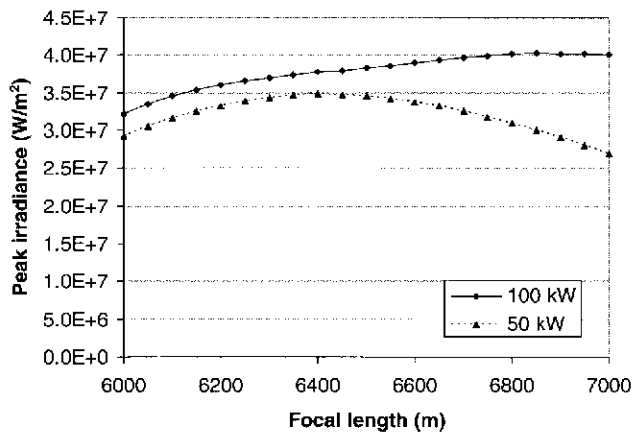

Fig. 1. Sensitivity of peak irradiance to focal range for baseline scenario.

screens were required to improve accuracy. Table 1 shows the effect of increasing the phase screen numbers for the baseline scenario (at 150 kW, for conservatism). Even though the average change in target peak irradiance by going from 20 to 30 phase screens was only 1.5% across the range of focal lengths considered (6–7.5 km), the change was more than 4% at some of the defocus values of interest. As a result, we used 30 phase screens in the wave-optics runs to determine laser system performance for the baseline scenario and variations from it. Further, in all scenario variations the position of the screens was biased in distribution toward the target, i.e., not uniformly distributed. For more details of this phase screen analysis, see Long.[11]

Wave-optics calculated performance results for the baseline scenario are shown in Fig. 1, which plots the peak irradiance at the target as a function of focal length. These peak irradiance values are averaged over 100 ms of dwell time after waiting 30 ms for the thermal blooming transient to settle. Since no turbulence is assumed, the averaging primarily has the effect of suppressing any remaining transient effects. For the 50-kW case, the optimal focal range is approximately 6.4 km, representing a defocus of 7% relative to the 6-km target range, and the optimal peak irradiance is about 19% higher than the peak irradiance for the focused beam. For the 100-kW case, the optimal focal range is approximately 6.85 km, a defocus of about 14%. In this case, the peak irradiance increases by 25% at the optimum focal range compared to the focused beam. In addition to the improvement in peak irradiance, it is noteworthy that the response curves under defocus are relatively

flat at the optimum operating points. This suggests that if a pattern can be determined for optimal defocusing, it may be relatively robust to uncertainties in the knowledge of driving parameters and therefore have utility in an operational environment. However, we note that this observed "flatness" appears to be sensitive to the obscuration assumption, discussed later. Next, we examine variations from baseline scenario in several dimensions and the effect on peak irradiance.

4. Power Sensitivity

In this section, the baseline scenario is expanded by looking at two laser power levels higher than 50 and 100 kW, from which we already saw a relationship between the optimal focal range and power. Figure 2 shows the peak irradiance functions for the baseline scenario at 150 and 200 kW under no turbulence and for 200 kW with HV 5/7 turbulence.

Notice that the peak irradiance functions with no turbulence are multimodal. However, it is interesting that the first peak is washed out by turbulence, as shown by the third line in Fig. 2. The peak that is washed out occurs in one of the secondary lobes of the irradiance pattern, which under our 30% central obscuration assumption are somewhat prominent in the diffraction limit, much more so than were the secondary lobes in the 10% obscuration cases considered below. Note that the optimal focus distance is about the same for the 200-kW case regardless of the turbulence assumption (not counting the first mode for the no-turbulence case). This result was true in general for the 30% obscuration cases across the power and range settings explored herein, but for the 10% obscuration, optimal defocus distance under turbulence is usually less than in the no-turbulence case due to strong interaction between thermal blooming and turbulence. Also, for the 30% obscuration, higher-order behaviors of the peak irradiance early in the defocus range are typically washed out by HV 5/7 turbulence. Therefore we use the location of the second maximum in these cases as the optimal focal range. Note that the optimal focal range continues to increase with power (and therefore N_D) for the baseline scenario.

Critical power is defined as the power at which peak irradiance no longer rises when power is increased. Figure 3 shows the peak irradiance for the baseline scenario as a function of

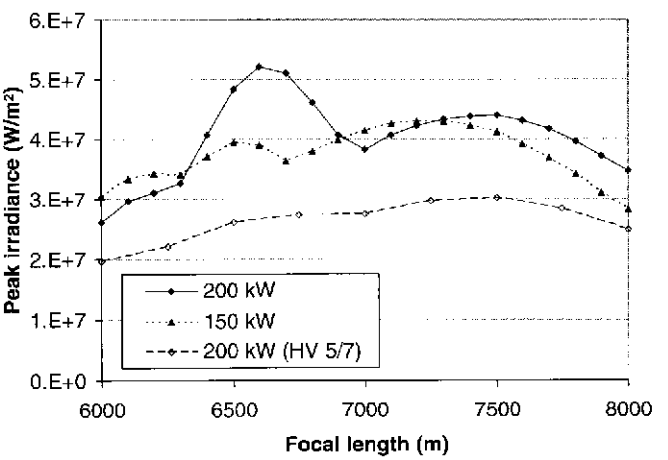

Fig. 2. Sensitivity of peak irradiance to focal range for baseline scenario at higher laser powers.

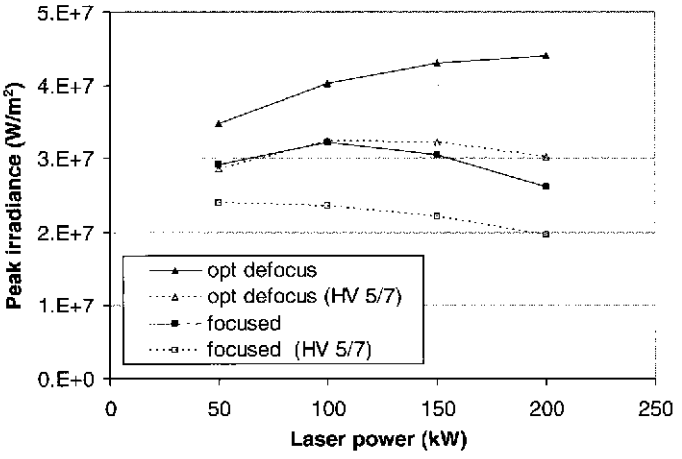

Fig. 3. Peak irradiance as function of laser power by focus and turbulence assumptions.

power for four different settings: focused beam and optimally defocused beam, each with no turbulence and with HV 5/7 atmospheres. From the no-turbulence (solid) lines in Fig. 3, it can be seen that critical power goes approximately from 100 kW for the focused case to 200 kW for the optimally defocused case. With-turbulence (dashed) lines suggest that the critical power goes approximately from 50 to 125 kW for the same change in paradigm. The fact that the critical power point decreases with the inclusion of turbulence indicates the existence of a positive interaction in Strehl ratio space between turbulence and thermal blooming. This will be addressed later. Next we look at the obscuration size dimension.

5. Obscuration Size Sensitivity

The central obscuration at the aperture represents an interesting dimension of the air-to-ground thermal blooming problem that we address next because its interaction with other dimensions will be also be discussed in subsequent sections. Here we investigate the baseline scenarios with the modification of assuming a 10% single-axis central obscuration, which represents an 8.8% increase in the area of the propagating aperture over the 30% obscuration case. The peak irradiance functions with respect to defocus for the baseline scenarios at both obscuration sizes are shown in Fig. 4. Note that the focused and optimal irradiances are all higher than for the 30% obscuration case and that the optimal focal length is shorter, especially for the 100-kW case. Some of this increased performance can be attributed to increased aperture area, but this cannot be said for the qualitative difference in defocus function, for which optimal performance occurs at 5% and 6.7% for the 50- and 100-kW cases, resulting in 22% and 42% increases in peak irradiance, respectively. The relative shortness of the optimal defocus distance remains in the 150- and 200-kW cases as well.

Figure 5 gives the irradiance plots for 150 and 200 kW and 10% obscuration, along with the turbulence case for 200 kW. The performance with no turbulence is significantly better than for the 30% obscuration case, and the optima occur at shorter focal ranges, 6.7% and 8.3%. However, under HV 5/7 turbulence in the 200-kW case a significant interaction with thermal blooming onsets, resulting in a shortening of the optimal focal range to 5% and a reduction in performance to slightly less than in the 30% obscuration case under turbulence. This interaction is similar to the one that washes out the high-order behavior

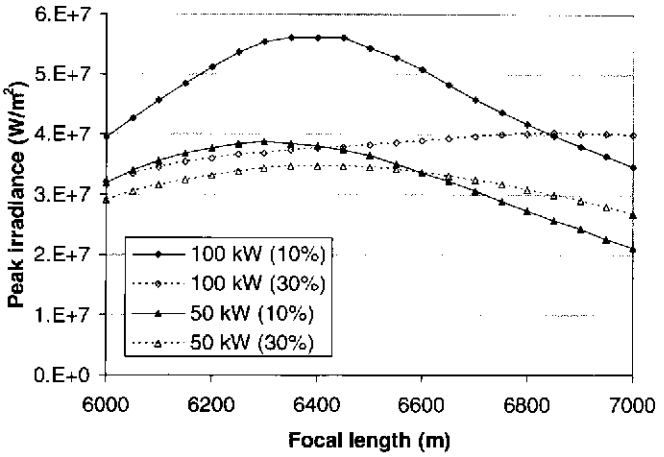

Fig. 4. Sensitivity of peak irradiance to focal range for baseline scenario with 10% and 30% central obscurations.

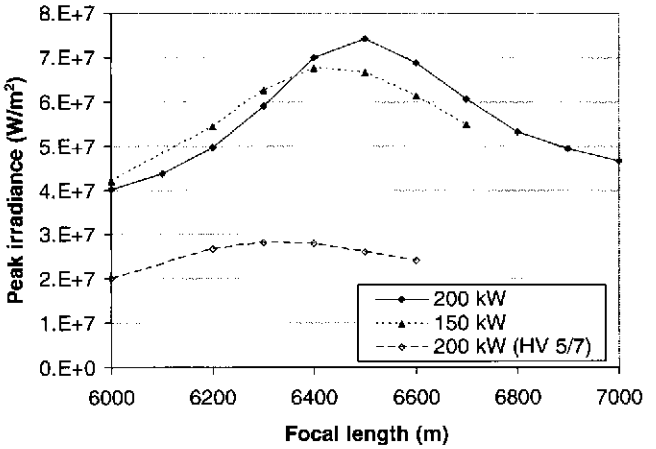

Fig. 5. Sensitivity of peak irradiance to focal range for baseline scenario with 10% obscuration at higher laser powers.

of the peak irradiance functions at 30% obscuration, but the 10% obscuration function is not bimodal. It is unclear why the 10% obscuration case should suffer so severely from the interaction at optimal performance under turbulence. The effect of this phenomenon is that optimal defocus with a 10% obscuration under turbulence will be slightly less than that for no turbulence.

6. Other Dimensions of Sensitivity

Rather than plot the irradiance functions with respect to focal length for all dimensions of interest, we resort to the Breaux distortion number N_D, which, in the focused case, is a useful function of the scenario variables. The 100-kW baseline scenario values are fixed for all dimensions except one, and values for the dimension of variation we evaluate are listed in Table 2 along with the Breaux N_D value for that scenario. This makes the 100-kW

Table 2. Scenario values and associated Breaux N_D for this study

Scenario description dimension to vary	Variation value	N_D
Power, kW	50	11.8
	100*	23.7*
	150	35.5
	200	47.3
Slant range, km	3	9.6
	4.5	16.6
	6*	23.7*
	9	37.2
Absorption (Table 3)	80% winter*	23.7*
	80% summer	53.5
Ground wind, m/s	2.5	41
	5	32.7
	10*	23.7*
Propagation vector	Perpendicular	9.8
	Parallel*	23.7*
Altitude, km	2*	23.7*
	3	16.6
	4	12.5

*100-kW baseline scenario (pivot point).

baseline scenario a pivot point from which we evaluate the sensitivity of performance in only one dimension of variation at a time. Then the optimal defocus multiples and irradiance improvement factors are plotted in Figs. 6–9 against Breaux N_D for all dimensions explored in this study. This approach also illustrates the utility of Breaux N_D as a predictor of optimal defocus and expected improvement.

The absorption dimension is not single valued, since it is a function of altitude, and we also include with it extinction due to scatter. Table 3 contains the combined molecular and aerosol absorption and scattering coefficients for the baseline (Mani) assumption and the 80-percentile summer case. The Mani atmosphere constitutes an approximately 80-percentile winter case. Note that the scattering (which is primarily due to aerosols) is left approximately unchanged between the cases.

The propagation vector warrants explanation also. The baseline scenario calls for the HEL platform to be flying toward the target. In this case, a component of the optical path (the propagation vector) is parallel with the velocity vector, and will be referred to as "parallel" propagation, though of course there is an angle between the propagation vector and the velocity vector in the baseline scenario since the laser is shooting toward the ground while the aircraft is flying level. "Perpendicular" propagation refers to a geometry in which the velocity vector is 90 deg from the propagation vector, meaning that the HEL is shooting to the side while flying into the wind. This geometry maximizes the effective wind velocity (due to aircraft motion and real wind) through the beam path; hence the significant reduction in N_D. On the other hand, turbulence losses in this geometry are greater, since the ability of a fast steering mirror to compensate for the higher-bandwidth tilt turbulence will be further taxed. Also, shooting to the side is anticipated to have some aero-optic beam spreading/distorting effects due to buildup of turbulence across the aperture glass that we do not model here.

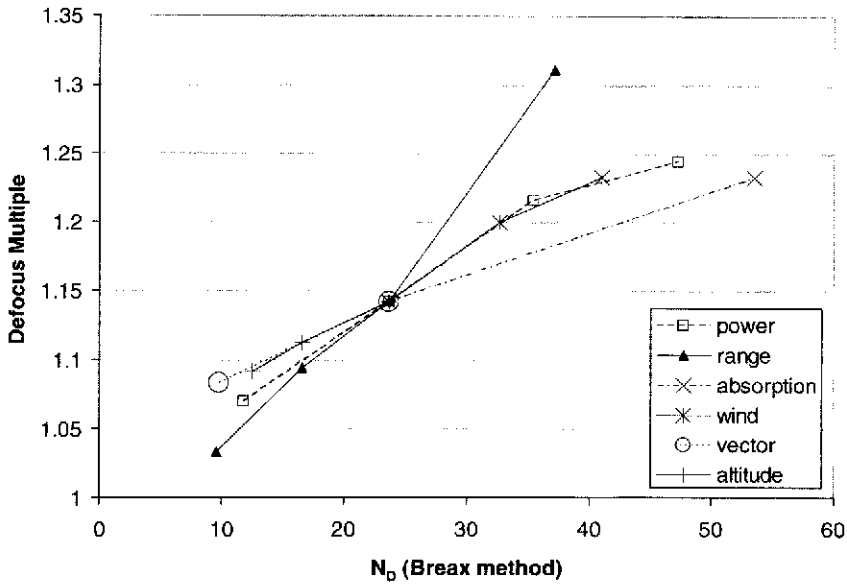

Fig. 6. Optimal focal length multiple of slant range (defocus) for 100-kW baseline scenario (30% obscuration) and varied parameters, as function of focused-case N_D.

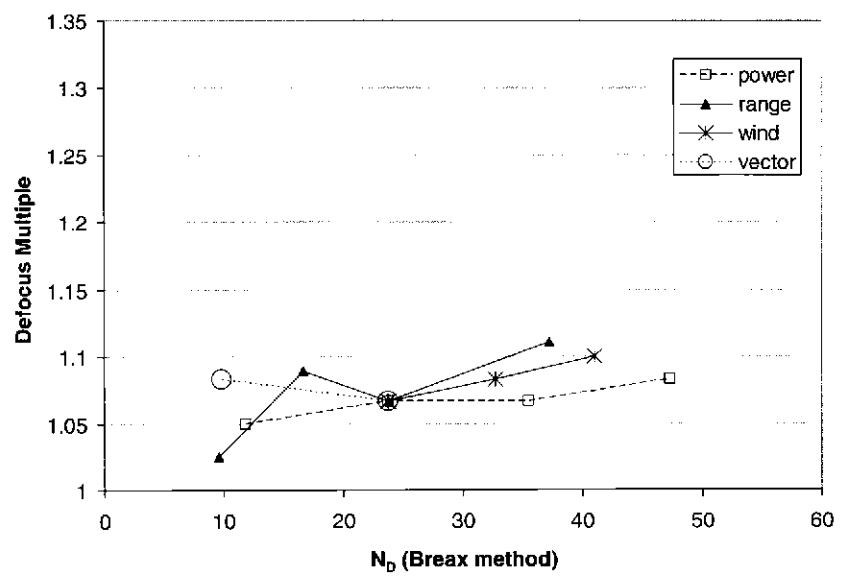

Fig. 7. Same as Fig. 6 except for 10% obscuration.

7. Optimal Defocus Performance by Obscuration Size

Using Breaux N_D as the independent variable, we plot the optimal defocus multiple (optimal focal range divided by R_{target}) and performance improvement factor (optimal peak irradiance divided by focused-case peak irradiance) for the baseline scenarios as well as

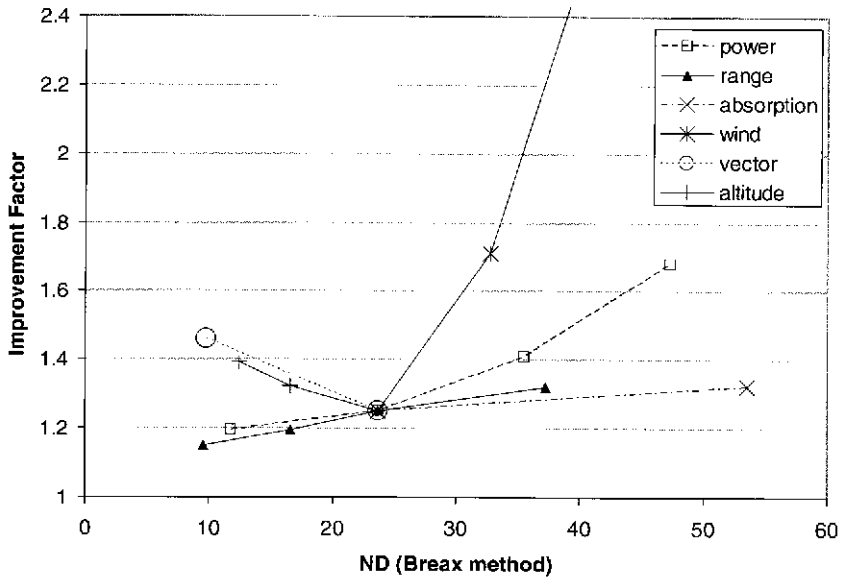

Fig. 8. Peak irradiance improvement at optimal defocus for 100-kW baseline scenario (30% obscuration) and varied parameters, as function of focused-case N_D.

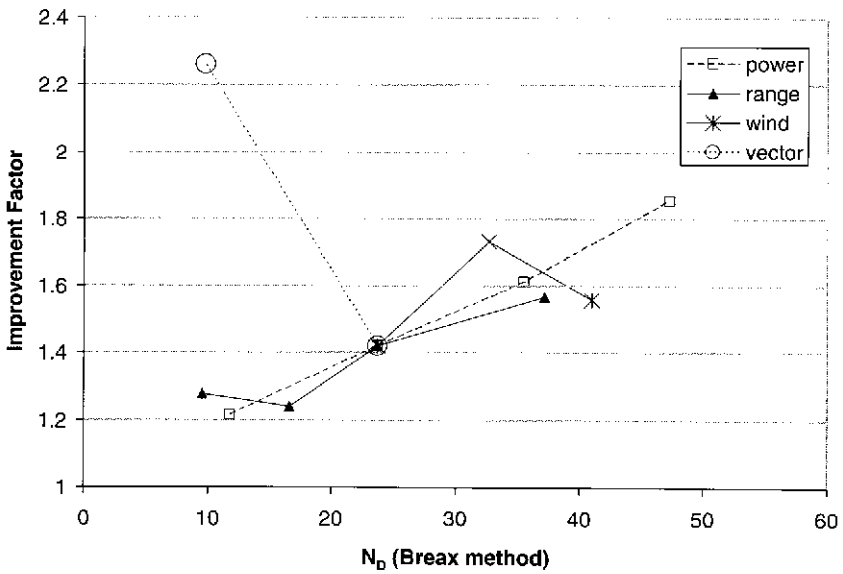

Fig. 9. Same as Fig. 8 except for 10% obscuration.

their variations, and we see that a relationship is apparent. Further, as suggested earlier, a clear distinction in that relationship appears between the 30% and 10% obscuration cases. Figures 6 and 7 show the respective optimal defocus multiples as a function of Breaux N_D for each dimension of variation. (Some of the dimensions were not explored for the

Table 3. Combined absorption and scattering coefficients due to molecular and aerosol effects in this study

Atmosphere	Altitude, km	α_{abs}	α_{scat}
Mani (80-percentile winter)	0	0.03755	0.05376
	1	0.01905	0.02377
	2	0.00827	0.00702
	3	0.00401	0.00305
	4	0.00199	0.00169
80-percentile summer	0	0.06681	0.05376
	1	0.06226	0.02377
	2	0.02103	0.00701
	3	0.01187	0.00304
	4	0.00656	0.00168

10% case since it was not the baseline scenario.) For the 30% obscuration, the optimal defocus appears to rise about 6% per $\Delta N_D = 10$, until about $N_D = 30$, when the defocus multiple rolls flat at about 1.25. In contrast to that, the optimal defocus multiple for the 10% obscuration jumps about 5% immediately and stays between 1.05 and 1.10. (Note that Figs. 6 and 7 have the same vertical scale for comparison purposes.) For the 10% obscuration case, given its susceptibility to turbulence interaction, it appears that one could safely operate at about 5% defocus at all times to get most of the defocus benefit and stay to the left of the optimal point.

Next we look at the peak irradiance improvement over the focused case as a function of N_D when operating at the optimal defocus shown above for each scenario. Figures 8 and 9 plot these results for the 30% and 10% obscuration cases, respectively, and as before, they have the same vertical axes to facilitate comparison. Figure 8 shows that the improvement in peak irradiance for the 30% obscuration case is a factor of 1.2 for many settings that span the N_D range. Exceptions are wind and power, the former of which shows large improvements, but that is primarily due to the fact that the slow winds significantly knock down S_{TB} (as shown in Fig. 10). This highlights the importance of wind as a major factor in determining a COIL-equipped ATL's performance, and when wind is low, defocusing the beam can offer significant assistance. (The improvement factor value that exceeded the vertical axis range on the wind line is 2.7 for $N_D = 41$.) Similarly, 200-kW power pushes down S_{TB}, making the recovery due to defocus look remarkable when in fact defocus is merely moving the critical power from a smaller value from 125 to 200 kW, as was shown in Fig. 3. The altitude and propagation vector lines illustrate better operating scenarios than the baseline scenario. Not only does propagating perpendicular to the velocity vector improve S_{TB}, as shown in Fig. 10, but that geometry also responds to defocus more readily. The same is true for increased altitude (keeping slant range the same). Combining the two geometries should yield additional benefit.

Figure 9 shows that despite the fact that the optimal defocus multiple is fairly flat for the 10% obscuration case (Fig. 7), the improvement over the focused case increases as Breaux N_D increases by about 18% per $\Delta N_D = 10$. It must be remembered that for the 10% obscuration, the larger improvements at high N_D will be offset by the thermal blooming-turbulence

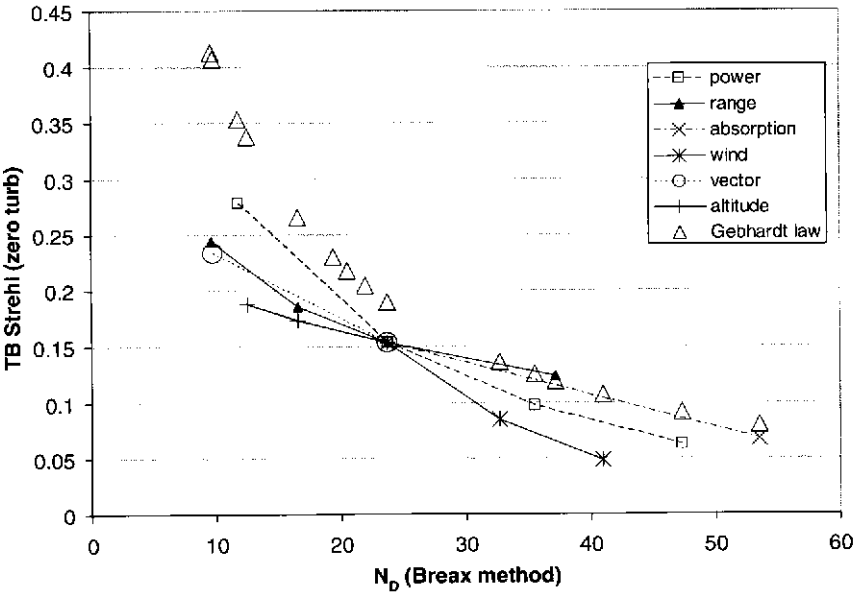

Fig. 10. Breaux N_D exhibits some inconsistency across the scenario variables in its correlation to S_{TB} for the air-to-ground case. Pivot point is baseline scenario at 100 kW.

interaction that affects this case to a greater degree, as we will show below for the case of laser power. The perpendicular propagation geometry again represents a better operating point than the baseline scenario and shows tremendous potential benefit from defocus; however, the interaction with turbulence will affect it also.

Wallace and Pasciak[20] found that in the case of the thermal lens being strongest close to the target plane, the amount of potential correction by adjusting the phase at the aperture is limited to about a factor of two. As discussed above, the air-to-ground case results in such a thermal lens placement. We have found that defocusing the beam, in every air-to-ground geometry explored here, results in some irradiance benefit. In many of the cases, a significant portion of Wallace's recovery limit is realized with defocus alone. The improvements found herein are also consistent in magnitude with findings by Pearson[15] for thermal lenses near the target plane.

Defocus appears to work, not because it constitutes a phase correction (most of the distortion being corrected with the small amount of focus we suggest is in the far-field portion of the focused beam), but rather because it reduces the beam spreading transverse to the wind that occurs near the target plane. An intense focused beam with a wind perpendicular to it will set up steep temperature gradients in the beam path that constitutes a negative lens and spreads the beam transverse to the wind. A small amount of defocus affects only the beam near the target, but this slightly wider beam with the same wind will have shallower temperature gradients, resulting in less spreading. To be sure, in the nonthermal blooming case defocusing the beam results in a decrease in peak irradiance, to which the improved S_{TB} is in effect applied. However, the strength of the negative thermal lens, even as close as it is to the target plane, is reduced at a faster rate than is the unbloomed irradiance for some amount of defocus. This view of the effect is supported by an experiment performed by

Edwards[4] in which he showed that jitter transverse to the wind was equivalent to defocus in improving irradiance of focused thermally bloomed beams. Yeh et al.[22] show that attempts to soften the transverse wind temperature gradient with "guide beams" improves irradiance. Finally, when observing the laser spot produced by our wave-optics runs, the classic thermal blooming crescent thickens as a function of defocus, and eventually a round core will emerge in the center of the crescent as the flattened temperature gradient allows the center of the beam to pass without spreading. This final effect usually occurs beyond the optimal defocus value, but its progression as a function of defocus supports the causal theory offered above.

8. Thermal Blooming Strehl

Thermal blooming Strehl S_{TB} is defined as the ratio between peak intensity of a beam with blooming distortion operative and the same beam with blooming distortion inoperative, but including extinction effects due to absorption and scatter. Smith[18] and Gebhardt[7] report good correlation of S_{TB} to N_D, and Gebhardt provides the following scaling law for uniform beams:

$$S_{\mathrm{TB}} = 1/\left(1 + 0.09N_D^{1.2}\right). \tag{4}$$

Figure 10 shows the resulting S_{TB} from the variations described in the preceding section. Each line represents a different dimension of variation, and the pivot point at $N_D = 23.7$ is the baseline scenario. All points in Fig. 10 are focused cases. The open triangles are a plot of Eq. (4), and it appears that the variation of S_{TB} as a function of N_D due to power variation is the closest to its shape, although there are reasons to expect that the Gebhardt law[7] would not match our wave-optics results: he uses a different formula for N_D that has no lever arm in the numerator or spreading function s. Ideally, a scaling variable would be constructed such that the slope of all the S_{TB} functions is the same near a common starting point; this would imply that the scaling relationship between the scenario dimensions had been captured. Where the line plots in Fig. 10 do not exhibit a common slope at the pivot point suggests where improvements in the Breaux N_D could be made for application in an ATL scaling law. The higher slope of the power S_{TB} line and still higher slope of the wind S_{TB} line relative to the other lines point to an inconsistency in the scaling variable and suggest that power and wind are not receiving enough weight relative to the other factors in the N_D calculation (or similarly that the other factors are receiving too much weight). The flatness of the nonwind and nonpower lines led Vernon and St. John to develop a transform for N_D for the other factors, as determined by Eq. (1), that remaps them more closely to the N_D response due to power (for the air-to-ground case).

Figure 11 contains all the same data as Fig. 10 but with the lines removed and the Gebhardt law highlighted with a dotted line. Added in are the S_{TB} lines for defocus as a function of N_D, the latter calculated in two different ways. One added plot (solid line, filled diamonds) is Breaux N_D calculated for defocus using Eq. (1), where a_{geom} is modified to represent increasing the focus distance beyond the target by 5%, 10%, and 15%: longer focus distances for the given target range increase S_{TB}. The large difference in slope between this plot and the rest of the S_{TB} functions indicates that the Breaux formulation (1) alone is not constructed in a way that allows N_D to be calculated for the defocused case. As mentioned earlier, the reason for this lies in Breaux's special spreading function s that is RSSed with a_{geom}. The second added plot (dash–dot line, filled boxes) in Fig. 11 is the S_{TB} function for

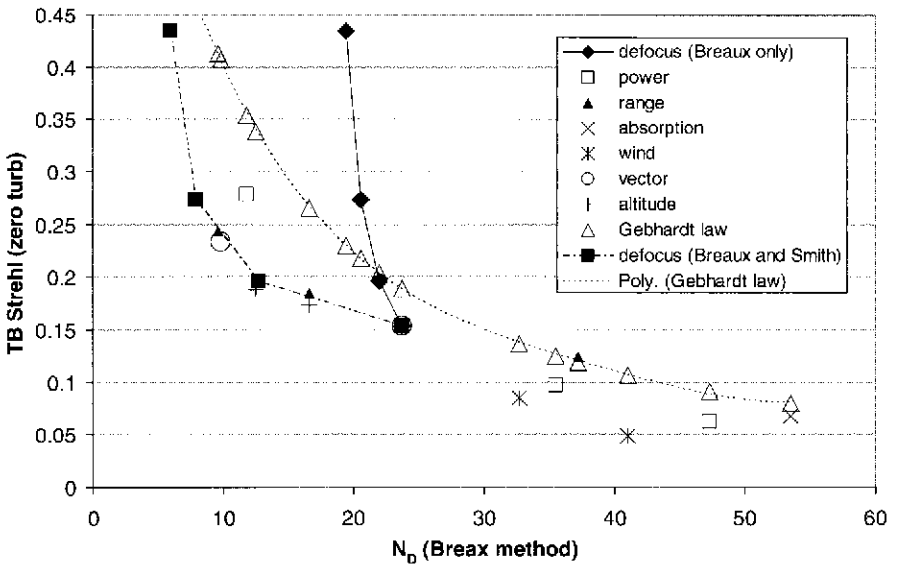

Fig. 11. Use of Smith correction factor removes gross inconsistency in Breaux N_D with respect to defocus scaling. The dashed "Poly" line is a fit to the Gebhardt law points to distinguish them from the scenario excursions. Pivot point is baseline scenario at 100 kW.

the same defocus values with N_D calculated by applying the Smith correction factor (3) to the Breaux N_D for the focused case. Interestingly, this approach yields an S_{TB} function that not only is more consistent with that of the other factors than is the solid, filled-diamond line, but is in fact very consistent with the nonpower, nonwind factors to the left of the pivot point. This result suggests that those thermal blooming scaling law models that depend on the Breaux technique for calculating N_D can capture the defocus effect in the scaling relationship by use of the Smith correction factor.

9. Effect of Turbulence

As mentioned in connection with Figs. 3 and 5, some scenarios that we study suffer from an interaction between turbulence and thermal blooming that reduces peak irradiance beyond what either effect would cause if applied independently. Not all such interactions will be detrimental to peak irradiance. Smith points out that if the bandwidth of the turbulence is higher than that of the thermal blooming process, the beam gets spread out in a time-averaged sense, resulting in less thermal blooming than would have otherwise occurred. All of the blooming discussed to this point is known as whole-beam blooming. However, at higher N_D, a small-scale blooming known as stimulated thermal Raleigh scattering (STRS) can emerge.[7] According to Chambers et al.,[3] this effect is caused by local focusing in the beam path due to the turbulence structure, which leads to inhomogeneous heating down the optical path and additional spreading due to the thermal lens caused by the uneven irradiance. This effect is captured in ACS, the model used in this study. For completeness, we mention Yahel,[21] who theorizes about a different kind of interaction in which the laser-induced temperature gradient in the beam path causes a new and more

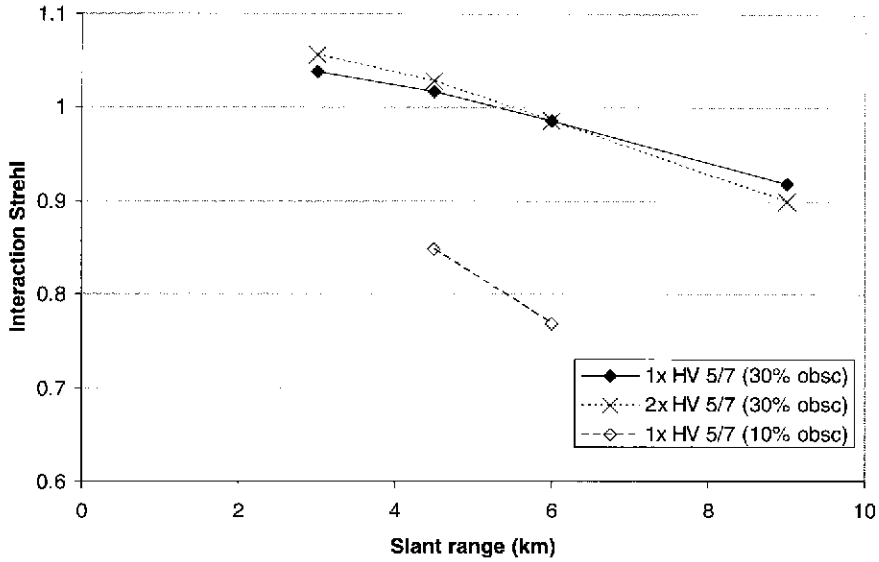

Fig. 12. S_{interact} for baseline scenario (100 kW) by turbulence multiple and obscuration size as function of slant range.

severe turbulence structure to arise. This effect is not captured in ACS, nor is it clear that his theory would apply to an ATL case, but if realized, it would be devastating to COIL ATL performance.

To develop scaling law models for defocus, it will probably be necessary to include not only a predictive variable for S_{TB} as a function of defocus, but also the interaction Strehl, since we find that it can be a significant component of the air-to-ground performance degradation. We will look at the interaction as a function of range for the 30% obscuration and then as a function of power for both obscurations, and finally we will look at perpendicular propagation.

Figure 12 shows the baseline scenario (100 kW) thermal blooming and turbulence interaction Strehl for the 30% obscuration case as a function of range at the optimal focal length for each range. This calculation for each scenario requires running the model for three cases: turbulence only, thermal blooming only, and both effects simultaneously. The interaction Strehl S_{interact} is then calculated by

$$S_{\text{interact}} = S_{\text{TB+turb}}/(S_{\text{TB}} S_{\text{turb}}). \tag{5}$$

Note that for the shorter ranges S_{interact} is actually greater than one, but that it drops below unity and decreases with range. The S_{interact} function is plotted for two levels of turbulence (1 and 2× HV 5/7), and note that for worse turbulence, the effect whether positive or negative appears to be amplified. None of these 30% obscuration interaction effects is terrible, especially compared to the 10% obscuration results on the same graph, which are at the optimal defocus setting for the with-turbulence assumption. Note that the vertical axis in Fig. 12 does not have zero at the origin.

Figure 13 shows S_{interact} for both obscurations as a function of power for the otherwise baseline scenario at optimum focal length. Here the greater sensitivity of the 10% obscuration case to interaction is clearly seen. Remember, however, that the 30% obscuration case

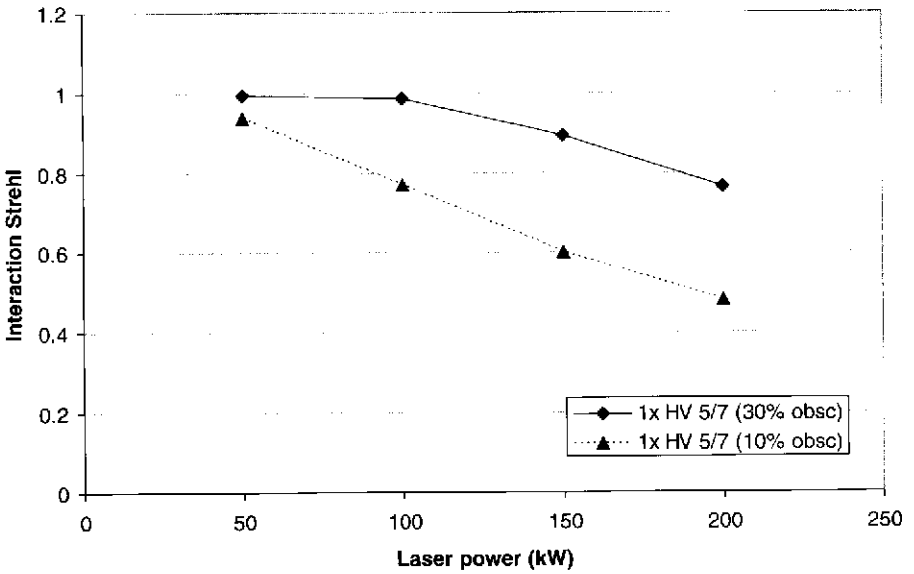

Fig. 13. S_{interact} at optimum defocus for baseline scenario by obscuration size as function of laser power.

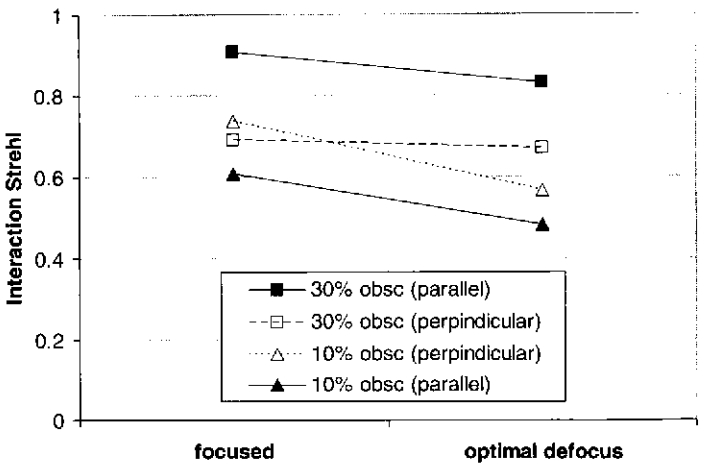

Fig. 14. S_{interact} for parallel and perpendicular propagation as function of focus setting at 200 kW for otherwise baseline scenario.

experiences these levels of interaction for some defocus values as well (e.g., the washed-out, higher-order peaks in Fig. 2), just not at the optimum defocus. The values for the 30% obscuration case update results presented by Long and Miller[12] for the interaction Strehl as a function of power. In that presentation, the interaction was overstated as a result of using too few phase screens in the simulation.

Figure 14 shows S_{interact} for both obscurations and both laser propagation vectors for the focused case and at optimal focal length. For both obscurations, S_{interact} is significant,

though it remains worse for the 10% obscuration at optimal defocus. So for perpendicular propagation, S_{interact} is less than 0.7 at optimal defocus for both obscurations, and we noted that the perpendicular case is probably a preferred operating geometry. Additionally, we have already noted that S_{interact} is dynamic with respect to the defocus multiple, and as such, it can alter the optimal defocus value from the no-turbulence case. The ability to predict a near-optimal defocus for ATL-like scenarios without having to directly measure the beam at the target will depend on our ability to understand the significance of STRS for the engagement and possibly have a predictive model for it.

10. Conclusions

Computer simulation evidence has been presented that a high-energy COIL air-to-ground system can realize significant benefits simply by defocusing the beam during an engagement. This result is consistent with the maximum expected benefit of phase correction when the thermal lens is located near the target plane.[20] Further, the optimal defocus amount is proportional to the thermal blooming distortion number of the focused case.

The functional form of optimal defocus appears to be sensitive to the size of the central obscuration for the uniform beam, with the 10% obscuration having a fairly flat response to Breaux N_D. The obvious benefit of using defocus is that because it is a radial phase parameter, precise knowledge of the wind direction is unnecessary to implement it, unlike the use of coma and astigmatism, as suggested elsewhere.[6] Additionally, most systems could take advantage of this phenomenon without major hardware modification.

Another important aspect of defocus benefit is related to radial beam spreading due to diffraction from aerosol forward scattering. In the boundary layer, significant aerosol densities can occur, which not only contribute to thermal blooming and extinction, but can also cause beam spreading on the same order of magnitude as turbulence.[5,16,17] This spreading cannot be compensated for by phase changes at the aperture. However, such spreading will likely have the same effect as intentional defocusing on an HEL under thermal blooming conditions so that the effect of aerosol spreading will merely be to improve peak irradiance, as long as the spreading does not overshoot the optimal defocus. On the other hand, aerosol spreading can only negatively impact the peak irradiance of lasers that do not operate under thermal blooming conditions.

Similarly, if aero-optic effects at the turret cause a high-bandwidth beam spreading, it may be that the focused, thermally bloomed beam benefits from the spreading, or at least is not adversely impacted, favoring the already preferred larger angle between the propagation and velocity vectors that reduces N_D. Alternatively, if the aero-optic spreading is low bandwidth, then an interaction with thermal blooming similar to that with turbulence could arise, forcing a smaller angle to be selected.

If the defocus effect on thermal blooming ATL-like systems is to be utilized, the capability to capture the effect of defocus in scaling laws is needed for systems analysis. Currently, scaling laws that use the Breaux N_D equation (1) cannot adequately represent this phenomenon. One path to correcting this deficiency is the use of the Smith correction factor (3). Finally, scaling laws do not appear to have been developed that capture the interaction between thermal blooming and turbulence in the ATL regime. This appears to be more of an issue for the 10% obscuration than the 30% in parallel propagation but is significant for both in the case of perpendicular propagation.

11. Disclaimer

The views expressed in this presentation are those of the authors and do not necessarily reflect the official policy or position of the Air Force, the Department of Defense, or the U.S. Government.

References

[1]Bradley, L.C., and J. Herrmann, Appl. Opt. **13**(2), 331 (1974).

[2]Breaux, H.J., SPIE **195**, 192 (1979).

[3]Chambers, D.H., T.J. Karr, J.R. Morris, P. Cramer, J.A. Viecelli, and A.K. Gautesen, Phys. Rev. A **41**(12), 6982 (1990).

[4]Edwards, B., "Thermal Blooming Mitigation: Experimental Results," presentation, Directed Energy Professional Society, Modeling and Simulation Conference, March 2004.

[5]Fiorino, S., R. Bartell, G. Perram, Z. Manning, S. Long, M. Houle, M. Krizo, D. Bunch, and L. Gravely, "Critical Assessment of Relative Humidity and Aerosol Effects on Lower-Atmospheric High Energy Laser Engagement," presentation, Directed Energy Professional Society, Modeling and Simulation Conference, March 2005.

[6]Gebhardt, F.G., Optica Acta **26**(5), 615 (1979).

[7]Gebhardt, F.G., Proc. SPIE **1221**, 2 (1990).

[8]Gebhardt, F.G., and D.C. Smith, IEEE J. Quant. Elec. **QE-7**(2), 63 (1971).

[9]Kanev, F., V. Lukin, and L. Lavrinova, Appl. Opt. **37**(21), 4598 (1998).

[10]Link, D., *Atmospheric Compensation Simulation: Users Manual*, Science Applications International Corporation Document (11 August 2004).

[11]Long, S.N., "Development of a High Energy Laser Predictive Scaling Law for Average Power in an Aimpoint Area Under Thermal Blooming and Turbulence Conditions," Ph.D. Dissertation, Air Force Institute of Technology (2007; not yet published).

[12]Long, S.N., and J.O. Miller, "Thermal Blooming PIB Scaling Law Development for COIL HEL—Work to Date," presentation, Directed Energy Professional Society, Modeling and Simulation Conference, March 2005.

[13]Magee, E.P., and A.M. Ngwele, "ATMTools: A Toolbox for Atmospheric Propagation Modeling, User's Guide, Version 2.2," ATK Mission Research Corporation Document (15 April 2005).

[14]Mani, S., "Atmospheric Transmission Models," unpublished paper (2004).

[15]Pearson, J.E., Opt. Lett. **2**(1), 7 (1978).

[16]Sadot, D., A. Melamed, N. Dinur, and N.S. Kopeika, Waves Random Media **4**, 487 (1994).

[17]Sadot, D., S. Shamriz, I. Sasson, I. Dror, and N.S. Kopeika, Opt. Eng. **34**(11), 3239 (1995).

[18]Smith, D.C., Proc. IEEE **65**(12), 1679 (1977).

[19]Vernon, R., and R. St. John, "HELCOMES User's Guide," Science Applications International Corporation Document (25 August 2003).

[20]Wallace, J., and J. Pasciak, J. Opt. Soc. Am. **67**(11), 1569 (1977).

[21]Yahel, R.Z., Appl. Opt. **29**(21), 3089 (1990).

[22]Yeh, C., J.E. Pearson, and W.P. Brown, Jr., Appl. Opt. **15**(11), 2913 (1976).

The Authors

Dr. Robert T. Brigantic is a Research Scientist with the National Security Directorate at the Pacific Northwest National Laboratory. He retired from the U.S. Air Force in 2005 with 22 years of experience in weapon systems logistics, space operations with a focus on command and control systems for shuttle operations and space test systems, and strategic airlift transportation. Dr. Brigantic holds a Ph.D. in operations research from the Air Force Institute of Technology (AFIT), an M.S. in space operations from AFIT, and a B.S. in chemical engineering from Oregon State University. Dr. Brigantic also serves as an Adjunct Professor of Operations Research with Washington State University and AFIT.

Dr. Matt Goda is a Lieutenant Colonel in the U.S. Air Force and an Assistant Professor of Electrical Engineering at the Air Force Institute of Technology. He received a B.S. in

physics from the University of Rochester in 1989, an M.S. in electro-optics from Tufts University in 1996, and a Ph.D. in electrical engineering from the University of Arizona in 2002. He previously worked at the Electronic Systems Center, Hanscom AFB, MA, and the Air Force Research Laboratory's Directed Energy Directorate in Albuquerque, NM. His areas of interest include atmospheric turbulence, atmospheric modeling, and laser communications.

Lieutenant Colonel Scott N. Long, U.S. Air Force, is the commander of the Air Education and Training Command Studies and Analysis Squadron at Randolph Air Force Base, TX. He received his B.S. in applied mathematics from the U.S. Air Force Academy in 1989 and his M.S. in operations research in 1995 from the Air Force Institute of Technology (AFIT) and is currently an Operations Research Ph.D. candidate at AFIT. Lt. Col. Long previously worked in the Air Force Research Laboratory's Directed Energy Directorate as well as in space systems testing at the Air Force Operational Test and Evaluation Center.

Dr. J.O. Miller is a 1980 graduate of the U.S. Air Force Academy (USAFA) and retired from the Air Force as a Lieutenant Colonel in January 2003. In addition to his undergraduate degree from USAFA, he received an M.B.A. from the University of Missouri at Columbia in 1983, his M.S. in operations research from the Air Force Institute of Technology (AFIT) in 1987, and his Ph.D. in industrial engineering from the Ohio State University in 1997. Dr. Miller is the Director of the Center for Operational Analysis and an Associate Professor in the Department of Operational Sciences at AFIT.